J. Electrochem. Sci. Eng. **15(5)** (2025) 2808; http://dx.doi.org/10.5599/jese.2808

Open Access : : ISSN 1847-9286
https://pub.iapchem.org/ojs/index.php/JESE

Original scientific paper

Synergistic corrosion inhibition and controlled release of ascorbic acid from a layered double hydroxide composite for stainless steel

Amal Abdouli[1], Mohamed Amine Djebbi[1,2,✉] and Abdesslem Ben Haj Amara[1]

[1]*Laboratory of Resources, Materials & Ecosystem (RME), University of Carthage, Faculty of Sciences of Bizerte, Zarzouna, 7021, Tunisia*

[2]*Université de Lorraine, CNRS, Institut Jean Lamour, F-54000, Nancy, France*

Corresponding authors: ✉med-djebbi@hotmail.fr;Tel. (33) 07 45 53 70 74

Received: May 16, 2025; Accepted: July 1, 2025; Published: July 7, 2025

Abstract

This study investigates the anticorrosion performance of ascorbic acid (AA) intercalated into a MgAl layered double hydroxide matrix as a sustained-release system for protecting stainless steel. The AA/MgAl layered double hydroxides (LDH) composite was synthesized via the co-precipitation method, and its structural and morphological properties were characterized using X-ray diffraction, Fourier-transform infrared spectroscopy, scanning electron microscopy, transmission electron microscopy and nitrogen adsorption/desorption measurements. The intercalation of AA into the LDH structure enabled a controlled and sustained release, enhancing its protective effect in an aggressive acid environment. Electrochemical impedance spectroscopy revealed a significant improvement in corrosion resistance, with the inhibition efficiency converted into an equivalent release rate, reaching up to 70 % after 210 minutes of immersion in 1 M HCl. Kinetic analyses demonstrated that the release of AA followed a non-Fickian diffusion mechanism, ensuring prolonged protection. Additionally, density functional theory and Monte Carlo simulations provided insights into the adsorption mechanisms, highlighting strong interactions between AA and both the LDH matrix and the Fe steel surface. This combined experimental and theoretical approach highlights the potential of AA/MgAl LDH as an efficient, sustainable, and long-lasting corrosion inhibitor, providing a promising solution for industrial applications in harsh acidic environments.

Keywords

Steel surface; layered double hydroxide composite; ascorbic acid intercalation; anticorrosive performance; smart inhibitor delivery; density functional theory study

Introduction

In the current technological context, the selection of materials for industrial applications is of paramount importance and requires a methodical approach based on thorough and informed

analysis. The design engineer, tasked with this critical responsibility, must carefully evaluate a wide range of criteria, including the physical properties of materials, their durability, and their performance under specific mechanical and environmental constraints [1]. Among these considerations, corrosion resistance is a crucial factor, particularly for metallic structures. Corrosion, a natural and destructive interfacial phenomenon, manifests as the gradual degradation of metals when exposed to corrosive environments such as acidic, saline, or humid conditions [2,3]. This complex process, influenced by chemical, physical, and electrochemical factors, presents significant challenges to various industrial sectors, including construction, energy, automotive, and aerospace. The impacts of corrosion extend beyond economic losses due to equipment deterioration, encompassing risks to safety and the environment as well [4]. Consequently, the selection of materials with effective corrosion resistance, along with the implementation of tailored solutions such as advanced composites or corrosion inhibitors, is critical to ensuring the durability and reliability of industrial infrastructures, particularly in extreme conditions [5].

Stainless steel (SS) is recognized as one of the most versatile and widely used materials across various industrial sectors, due to its exceptional durability and corrosion resistance. Its popularity extends to key industries such as oil, chemicals, and food processing [6,7], where it is often exposed to extreme conditions. These environments include severe corrosive settings, exacerbated by essential industrial processes such as pickling, descaling, and acid cleaning. While these treatments are crucial for ensuring the cleanliness, functionality, and longevity of equipment, they also expose metal surfaces to increased corrosion risks, compromising their long-term performance [8]. In response to these challenges, the search for reliable protection solutions has led to the development and optimization of advanced methods, including the use of corrosion inhibitors. These inhibitors, which play a key role in protective coatings, aim to extend the lifespan of stainless steel structures by creating effective barriers against chemical aggressions [9,10].

Among innovative approaches for corrosion protection, layered double hydroxides (LDHs) have emerged as promising materials due to their unique ion-exchange properties and ability to host and release functional anions in a controlled manner [10-12]. LDHs, also known as hydrotalcite-like compounds, are composed of hydroxide layers formed by divalent (M^{2+}) and trivalent (M^{3+}) metal ions, imparting a positive charge to the layers. Interlayer anions (A^{n-}) and water molecules occupy the space between the layers, contributing to structural stability (Figure 1).

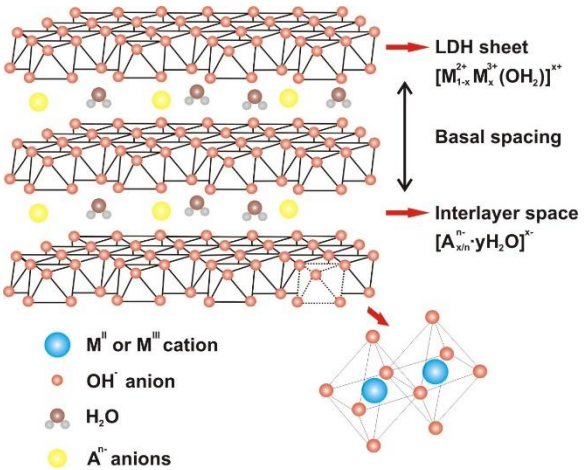

Figure 1. *Schematic structure of LDH*

The general formula for LDH can be expressed as $[M^{2+}_{1-x}M^{3+}_{x}(OH)_2]^{x+}[A^{n-}_{x/n}\cdot yH_2O]^{x-}$, where *x* represents the molar fraction of trivalent cations [13]. The layered structure typically exhibits a

hexagonal symmetry (space group R-3m), with structural parameters such as the *a* and *c* lattice constants influencing the material's properties. These features enable LDHs to capture aggressive anions from the environment and simultaneously release protective species, offering a dual functionality that is particularly attractive for smart corrosion protection systems [11-17].

While several studies have investigated the application of LDHs for corrosion protection of aluminium alloys and carbon steel [18-20], relatively few have addressed their use for stainless steel substrates. Most LDH-based corrosion protection strategies have focused on loading inorganic inhibitors, such as chromate [18], molybdate [21], or phosphate ions [22]. However, the intercalation of organic corrosion inhibitors into LDHs, particularly natural and environmentally friendly molecules like ascorbic acid, remains underexplored for stainless steel. Furthermore, achieving a controlled and sustained release of organic inhibitors from LDH matrices offers significant potential for enhancing long-term corrosion resistance while mitigating health and environmental risks.

In this context, ascorbic acid (AA), a naturally occurring, effective, and non-toxic corrosion inhibitor, represents a particularly attractive candidate. AA acts by donating electrons to metal surfaces, thereby reducing corrosion rates through the formation of protective films and the naturalization of aggressive species [23,24]. Its controlled release from a suitable host material could significantly improve the durability and efficacy of corrosion protection systems under harsh conditions [25]. Incorporating ascorbic acid into an LDH matrix could simultaneously leverage the barrier effect of the lamellar structure and the ion exchange capacity for prolonged inhibitor delivery, presenting a novel strategy for protecting stainless steel surfaces.

This study aims to evaluate the anticorrosion performance of AA intercalated into a MgAl-LDH matrix as a sustained-release system for protecting SS in a strongly acidic environment (1 M HCl). Although LDHs, including MgAl-LDH, are known to dissolve under such highly acidic conditions gradually, they are more commonly applied in neutral or saline media for corrosion inhibition. This work represents the first report exploring an LDH-based composite for corrosion protection under acidic attack, with an explicit investigation of the interfacial mechanisms involved. To this end, MgAl-LDH nanocarriers loaded with AA were initially synthesized *via* the co-precipitation method. Ascorbic acid was selected for its proven corrosion inhibition performance for stainless steel in aggressive environments [23], while its intercalation within the LDH lamellar structure was designed to enable controlled and prolonged release [26]. Structural and morphological changes induced by the intercalation process were characterized by X-ray diffraction (XRD), Fourier-transform infrared spectroscopy (FTIR), nitrogen (N_2) adsorption-desorption analysis, scanning electron microscopy (SEM), and transmission electron microscopy (TEM). The anticorrosion performance of the resulting composite was assessed using electrochemical impedance spectroscopy (EIS), and kinetic analyses were conducted to correlate the release profiles with the corrosion protection behaviour. Additionally, density functional theory (DFT) calculations and Monte Carlo (MC) simulations were employed to provide molecular-level insights into the interaction mechanisms between the LDH matrix, the encapsulated AA, and the SS surface. This integrated experimental and theoretical approach offers a comprehensive understanding of how the controlled release of AA contributes to corrosion resistance and how the LDH structure behaves before and during its dissolution in an acidic medium, thereby paving the way for the development of a novel and environmentally friendly strategy for industrial corrosion protection.

Experimental

Reagents and instruments

Magnesium chloride hexahydrate ($MgCl_2 \times 6H_2O$, 99.999 %), anhydrous aluminum chloride ($AlCl_3$, 99.99 %), sodium hydroxide (NaOH ≥ 98 %), hydrochloric acid (HCl, 37 %), and ascorbic acid ($C_6H_8O_6$) were acquired from Sigma-Aldrich and Fisher Scientific. Stainless steel 092-C specimens with chemical composition 18.0 wt.% Cr, 8.0 wt.% Ni, 2.0 wt.% Mn, 0.75 wt.% Si, 0.08 wt.% C, 0.045wt.% P, 0.030wt.% S and the balance Fe were used for the experiments.

The crystal structure of the samples was determined using X-ray diffraction (XRD) with a Bruker D8 Advance diffractometer, equipped with CuKα radiation (λ = 0.15418 nm). Data were collected over a 2θ range of 2 to70° with an angular step size of 0.02° and a counting time of 67.1 s per step. Functional groups involved in the co-precipitation process were examined through Fourier transform infrared (FTIR) spectroscopy in transmittance mode, using a Nicolet 2000 spectrometer. Spectra were recorded within the 4000 to 500 cm^{-1} range at a spectral resolution of 1 cm^{-1}. Microstructural features were analysed via scanning electron microscopy (SEM) and transmission electron microscopy (TEM) with Quanta 200 FEI and Tecnai G2 FEI microscopes, operated at 5 kV and 200 kV, respectively. The specific surface area was evaluated using the BET method, based on N_2 adsorption-desorption measurements conducted with a Micromeritics ASAP 2020 analyser.

Co-precipitation of MgAl and AA/MgAl LDHs

A 50 mL solution containing Mg^{2+}-divalent and Al^{3+}-trivalent metal salts, with a total concentration of 1 M and a molar ratio of Mg^{2+}/Al^{3+} = 2, is gradually introduced into a reactor filled with 50mL of deionized water under continuous magnetic stirring. The pH is maintained at a constant 9 by the simultaneous addition of a 2 M sodium hydroxide solution, controlled by an automated system equipped with a syringe pump and a pH meter, which precisely regulates reagent flow rates. To prevent contamination by carbonate ions from atmospheric CO_2, the synthesis is carried out under a nitrogen atmosphere at 25°C. The resulting precipitate undergoes multiple washing and centrifugation cycles with deionized water before being dried in air at room temperature.

Following a procedure similar to that used for the synthesis of reference MgAl LDH, the AA/MgAl LDH material was prepared *via* co-precipitation at a constant pH of 9. This process involved the simultaneous addition of a 0.1 M solution of metal salts, with a Mg^{2+}/Al^{3+} molar ratio of 2 and 0.2 M sodium hydroxide solution into an aqueous medium containing 1 g of ascorbic acid. The metal salt solution was introduced at a controlled flow rate of 0.12 mL/min. The co-precipitation reaction was carried out under a nitrogen atmosphere, and the resulting suspension was allowed to mature for 2 hours. The solid product was then isolated through successive washing and centrifugation cycles, followed by drying in ambient air.

Corrosion assays: electrochemical measurements

Electrochemical measurements were performed using a PC-controlled potentiostat/galvanostat (VoltaLab) equipped with VoltaMaster 4 software. A conventional three-electrode setup was employed, consisting of a 0.5 mm platinum wire as the counter electrode, a saturated calomel electrode (SCE) as the reference electrode, and an SS type 092-C working electrode with an active surface area of 1 cm^2. All electrochemical measurements were carried out in an aqueous 1 M HCl solution as the electrolyte. The open-circuit potential (OCP) of the stainless steel was monitored over time in the corrosive medium until it stabilized, ensuring that the system reached a quasi-equilibrium state. Electrochemical impedance spectroscopy (EIS) was then performed at the

stabilized OCP, using a 10 mV AC signal over a frequency range of 100 kHz to 0.1 Hz, without applying any external DC bias, assuming a time-invariant system during the measurement. The experiments were conducted with the stainless steel specimen in the presence of 1 g L^{-1} of the AA/MgAl LDH composite dispersed in the electrolyte solution.

Density functional theory study

Computational methods

To investigate the nature of interactions between MgAl-LDHs, Fe(110) surface of SS, and ascorbic acid, as well as to assess the energy modifications induced by intercalation, quantum chemistry calculations were carried out using density functional theory (DFT). These simulations were performed with various computational tools available in the Material Studio 2017 software package [27]. The study aimed to provide insights into the structural, electronic, and energetic changes occurring within the LDH framework upon ascorbic acid intercalation, offering a deeper understanding of the stability and bonding mechanisms at the molecular level.

Model construction and geo-optimization

A structural model of MgAl LDH with an atomic ratio of 2 was constructed using the modelling tools available in BIOVIA Materials Studio 2017 [27]. The model parameters were derived from X-ray crystallographic data of hydrotalcite, with a space group R-3m and lattice parameters $a = b$ = = 0.30729 nm, c = 2.3326 nm [28,29]. A supercell was generated by replicating the unit cell 3×3×1 along the (*X*, *Y*, *Z*) directions. Two distinct models were developed: the first represented a broad (003) double-layer surface, while the second featured a (010) cleaved surface, both embedded within a simulation box containing a 2.0 nm thick vacuum layer to prevent interactions with periodic images. Geometry optimization of both the LDH substrate and AA was performed using the FORCITE module [30,31], applying the UNIVERSAL force field with QEq charge equilibration [32]. Electrostatic and Van der Waals interactions were treated using an atom-based approach for ascorbic acid, whereas, for the substrate, Ewald summation [33] was used for electrostatics, while Van der Waals interactions were also modelled with an atom-based method.

Monte Carlo simulation

The interactions between the various MgAl-LDH surfaces, Fe(110) surface of SS, and ascorbic acid were analysed using the ADSORPTION locator module. The UNIVERSAL force field was employed with QEq charge equilibration. Electrostatic interactions were treated using the Ewald summation method, while Van der Waals interactions were modelled using an atom-based approach. Simulated annealing parameters were set to 10 cycles, each with 100,000 steps, to ensure accurate energy convergence. The adsorption energy was determined using Equation (1) [34]:

$$E_{ads} = E_{LDH/AA} - E_{LDH} - E_{AA} \quad (1)$$

where E_{ads} / kJ mol^{-1}represents the total energy of the AA adsorbed on the LDH surface, E_{LDH} / kJ mol^{-1} corresponds to the total energy of the LDH and E_{AA} / kJ mol^{-1}denotes the total energy of AA.

Density functional theory calculations

Density functional theory (DFT) calculations were carried out using the DMol³ module [27,30]. Energy calculations were performed using the generalized gradient approximation (GGA) method [32], combined with the Perdew-Burke-Ernzerhof (PBE) [28] functional and the Tkatchenko-Scheffler (TS) method for DFT-D corrections [35]. The double numerical plus polarization (DNP) basis

set was selected, with an all-electron core treatment and a Gamma K-point sampling. Additionally, the COSMO solvation model was applied, using water as the solvent [36].

To further validate the adsorption mechanism between the LDH structure, Fe(110) of SS, and ascorbic acid (AA), key electronic properties were analysed based on DFT calculations, including the HOMO-LUMO energy gap (E_{gap})**,** Mulliken charges**,** electron affinity (A), global hardness (η), softness (σ), absolute electronegativity (χ), electronic chemical potential (μ), back-donation energy ($\Delta E_{back\text{-}donation}$), and the electronic donation fraction (ΔN). These parameters provide insights into the electronic structure of the adsorbed species. The corresponding energy values were computed using equations (2) to (9) [37]:

$$\Delta E_{gap} = E_{LUMO} - E_{HOMO} \quad (2)$$

$$A = -E_{LUMO} \quad (3)$$

$$\eta = \frac{E_{LUMO} - E_{HOMO}}{2} \quad (4)$$

$$\sigma = \frac{1}{\eta} \quad (5)$$

$$\chi = \frac{-\left(E_{LUMO} + E_{HOMO}\right)}{2} \quad (6)$$

$$m = -\chi \quad (7)$$

$$\Delta E_{back\text{-}donation} = \frac{1}{8}\left(E_{HOMO} - E_{LUMO}\right) \quad (8)$$

$$\Delta N = \frac{\left(\chi_{Fe} - \chi_{AA}\right)}{2\left(\eta_{Fe} + \eta_{AA}\right)} \quad (9)$$

Results and discussion

Physico-chemical characterization of materials

The crystallographic properties of the synthesized MgAl LDH nanosheets and AA/MgAl LDH composite were analysed using powder X-ray diffraction (XRD)**.** Figure 2a presents the XRD pattern of the as-prepared MgAl LDH**,** which aligns with previously reported data [13,38]. The presence of sharp and intense diffraction peaks confirms its crystalline nature and corresponds to a hexagonal lattice with R-3m rhombohedral symmetry [39,40]. The characteristic (00l) diffraction peaks at 11.71°, 23.21°, and 35.11°, assigned to the (003), (006), and (009) planes, respectively, indicate the formation of the lamellar LDH structure. The d-spacing for the (003) plane (0.755 nm) suggests the presence of intercalated water and chloride ion**s**. The lattice parameter c was calculated using Equation (10):

$$c = 3/2[d_{003} + 2d_{006}] \quad (10)$$

Additionally, the reflection at 2θ= 61.25°, corresponding to the (110) plane, provides insights into the cation-cation distance, allowing for the calculation of the lattice parameter *a*, Equation (11):

$$a = 2d_{110} \quad (11)$$

Table 1 summarizes the crystallographic data for MgAl LDH. Upon interaction with AA bio-molecules, significant changes in the XRD pattern of the co-precipitated AA/MgAl LDH phase were observed (Figure 2b). The diffraction peak intensities decreased and became broader, particularly for the (001) reflection, which shifted to a lower 2θ (8.60°)**.** This shift corresponds to an increased *d*-spacing (0.925 nm), indicating an expansion of approximately 0.170 nm. Such an increase suggests the successful intercalation of AA molecules into the interlayer region of MgAl LDH. Moreover, the

notable reduction in peak intensities and their broadening in the AA/MgAl LDH composite likely indicate a decrease in particle size, as estimated using the Debye-Scherrer calculator (Table 1). These structural modifications indicate the onset of LDH layer exfoliation, resulting in a more uniform dispersion of biomolecules within the inorganic layers.

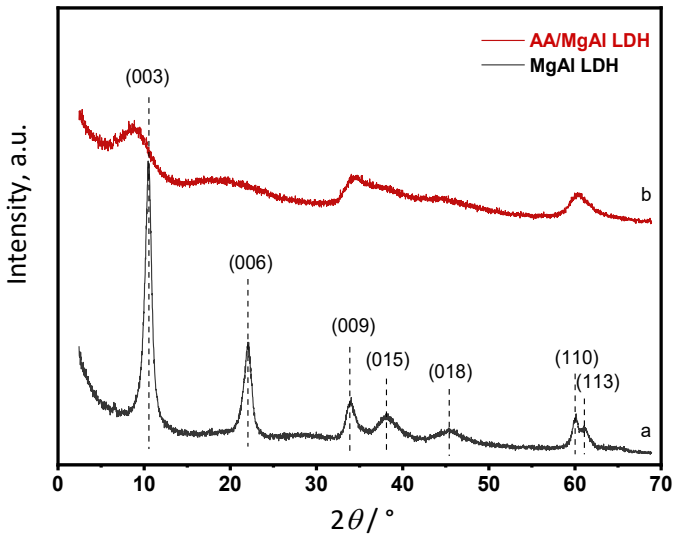

Figure 2. *XRD patterns of (a) MgAl LDH nanosheets and (b) AA/MgAl LDH composite*

Table 1. *Crystallographic data of MgAl LDH and AA/MgAl LDH composite, and specific surface area*

LDH	d_{003}/ nm	d_{110} / nm	Crystallite size, nm*	Lattice parameter		S_{BET}/ m^2g^{-1}
				c/ nm	*a*/ nm	
MgAl LDH	0.755	0.151	29.5	2.281	0.302	158.1
AA/MgAl LDH	0.925	0.150	14.0	2.775	0.300	-

* The crystallite size was calculated by the Scherrer calculator using PANalytical X'Pert HighScore Plus software from the full-width at half-maximum (FWHM) intensity of the (003) reflection

To further investigate the textural properties of MgAl LDH, N_2 adsorption-desorption measurements were conducted at 77 K. The resulting isotherm, presented in Figure 3, provides valuable insights into the porous structure of the material.

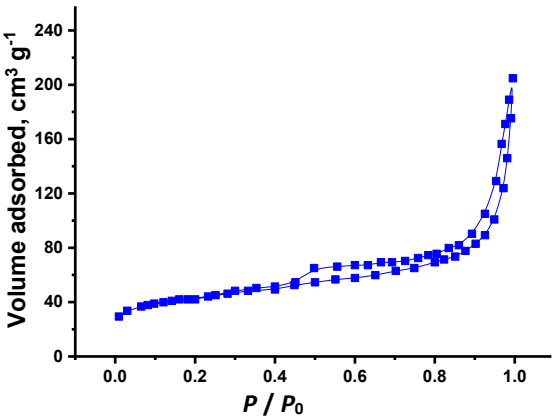

Figure 3. *N_2 adsorption-desorption isotherm illustrating the textural properties of the MgAl LDH phase*

Based on the IUPAC classification, the obtained isotherm exhibits a characteristic Type IV shape, which is indicative of mesoporous materials. A pronounced hysteresis loop is observed in the relative pressure range (P/P_o) of 0.4 to 1.0, confirming the presence of mesopores within the LDH structure. The Brunauer-Emmett-Teller (BET) analysis reveals that the specific surface area of the as-synthesized MgAl LDH reaches approximately 158.1 m^2 g^{-1} (Table 1). This relatively high surface

area suggests that the synthesized LDH phase possesses a well-developed porous network, making it a suitable host matrix for the incorporation and confinement of ascorbic acid molecules.

The functional groups present in MgAl LDH, the AA/MgAl LDH composite, and ascorbic acid molecules were analysed using FT-IR spectroscopy in transmittance mode. Figure 4a shows the FT-IR spectrum of MgAl LDH in the range of 4000 to 400 cm^{-1}. A broad and intense band at 3404 cm^{-1} is attributed to the stretching vibrations of hydroxyl groups originating from both brucite-like layers and intercalated water molecules. A standard region between 2750 and 1750 cm^{-1} corresponds to background noise. The bands observed in the mid-region are associated with the bending mode of water molecules (1636 cm^{-1}) and the vibrational mode of interlayer carbonate anions (1358 cm^{-1}), likely resulting from atmospheric CO_2 contamination that can transform into CO_3^{2-} ions and infiltrate the LTH interlayers [41]. Finally, the bands below 1000 cm^{-1} correspond to the intrinsic vibrations of tetrahedral and octahedral M-O (557, 654 and 761 cm^{-1}) and O-M-O (444 cm^{-1}) sites within the brucite layers [42].

Upon introducing AA biomolecules (Figure 4b), a slight shift in the intrinsic vibration bands of the LDH lattice was observed in the FT-IR spectrum of the AA/MgAl LDH composite, indicating the active involvement of AA molecules within the LDH matrix. Furthermore, the band at 1358 cm^{-1}, attributed to the stretching vibration of CO_3^-, completely disappeared in the composite spectrum after the co-precipitation reaction, suggesting that the interlayer carbonate and chloride anions were entirely exchanged by ascorbic acid molecules. The two bands at 1319 and 1267 cm^{-1} (Figure 4c), associated with AA functional groups, correspond to the vibrations of the lactone linkage (C-O-C) and the carbonyl group (C=O) [43,44]. These bands are slightly shifted to 1387 and 1319 cm^{-1}, respectively, which is likely due to the weakening of intramolecular hydrogen bonds upon intercalation.

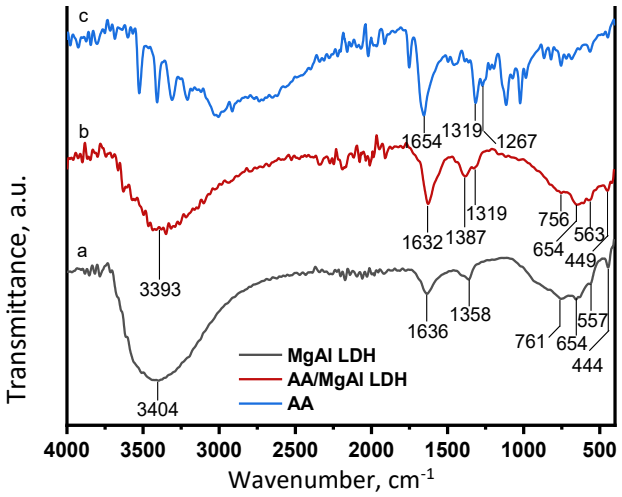

Figure 4. *FTIR spectra of (a) MgAl LDH nanosheets, (b) AA/MgAl LDH composite and (c) AA molecules*

Additionally, the weak bending mode of H_2O, observed initially at 1636 cm^{-1} in the FTIR spectrum of LDH, shifted to 1632 cm^{-1} in the AA/MgAl LDH composite spectrum. This shift may result from overlap with the broad and strong peak at 1654 cm^{-1}, attributed to conjugated C=C vibrations. Moreover, the band broadening after intercalation is likely due to electrostatic interactions between AA molecules and hydroxide layers, suggesting their stable incorporation into the interlayer space of LDH. This phenomenon, previously reported in other studies [45,46], is further confirmed by the FTIR data, which provide evidence of AA anion intercalation within the LDH structure.

The morphology and nanostructure of MgAl LDH nanosheets and the AA/MgAl LDH composite were analysed using SEM and TEM, respectively, as illustrated in Figure 5**.** As shown in the micrographs, MgAl LDH exhibits a near-spherical, platelet-like structure with dimensions ranging

from 50 to 500 nm (Figure 5a and 5b), forming agglomerates in a characteristic "sand rose" arrangement (Figure 5c), which is typical of hydrotalcite-like compounds [47].

However, upon the diffusion of AA molecules between the LDH layers, significant textural changes are observed. These include a reduction in crystallinity (Figure 5d and 5e) and a reorientation of crystallite stacking (Figure 5f). The co-precipitated biohybrid phase, therefore, displays an irregular morphology due to the non-uniformity of crystal growth along different crystallographic directions. The presence of a high concentration of biomolecules in the precipitate medium influences the material's morphology and disrupts its crystal growth process. These observations suggest that the extensive dispersion of AA molecules on the surface, edges, and within the mesopores enhances the cohesive interactions between AA molecules and the inorganic layers, ultimately leading to the exfoliation of the latter.

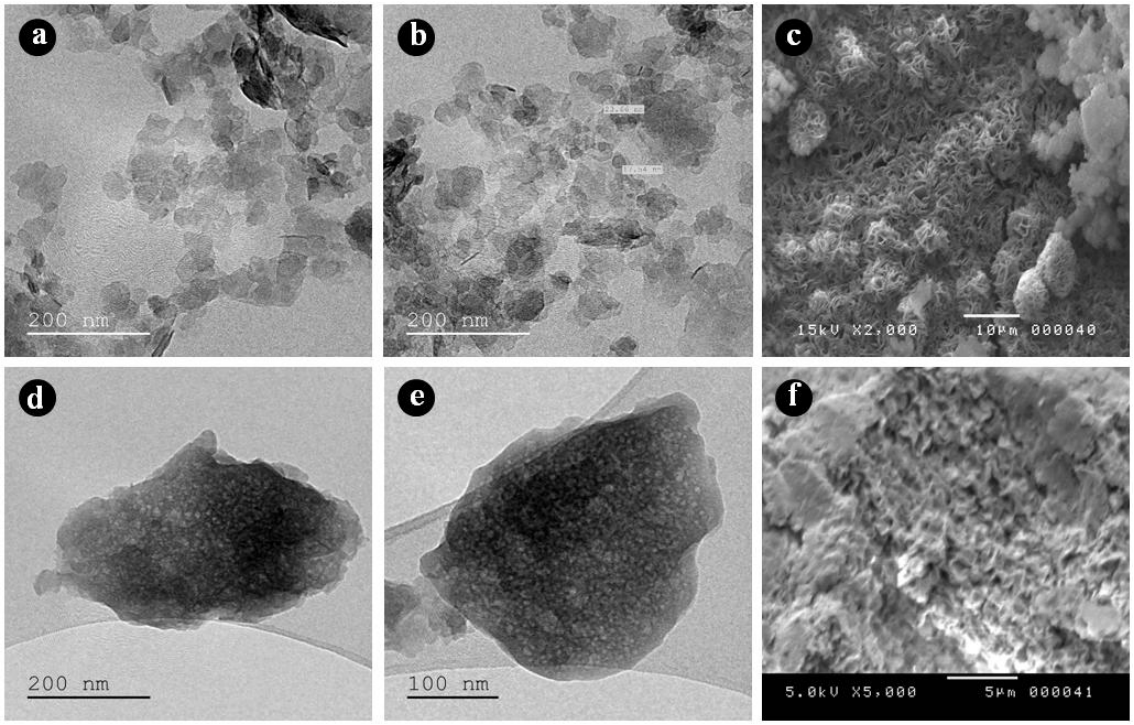

Figure 5. *TEM and SEM images of (a, b, and c) MgAl LDH nanosheets and (d, e, and f) AA/MgAl LDH composite*

Additionally, EDX analysis results are presented in Figure 6a, confirming that MgAl LDH is composed of magnesium, aluminium, and chloride.

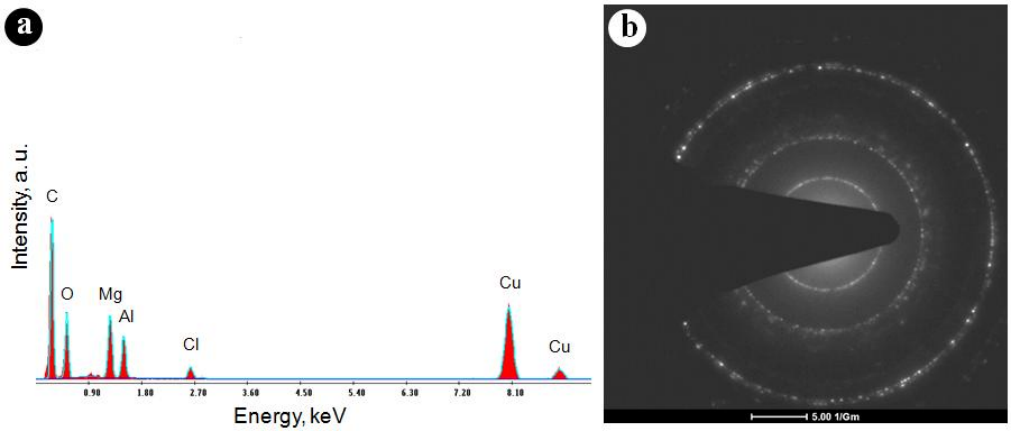

Figure 6. *EDX (a) and SAED (b) images of MgAl LDH nanosheets*

Elemental analysis based on semiquantitative EDX data indicates an atomic ratio of magnesium to aluminium of 1.94. The inset graph in Figure 6b displays the SAED pattern of the MgAl LDH nanoparticles, where the observed diffraction rings clearly indicate the high crystallinity of the sample. These rings can be indexed to hexagonal polycrystals and are attributed to the (001) LDH planes. The obtained results align well with theoretical computations based on XRD measurements.

Anticorrosion investigations

Figure 7 presents the Nyquist plots for stainless steel exposed to a 1 M HCl solution, both in the absence and presence of an AA/MgAl LDH composite at different immersion times. These measurements were conducted under open-circuit potential conditions to analyse the corrosion behaviour of the system. The Nyquist plots exhibit characteristic semicircular shapes across all conditions, indicating a charge transfer-controlled corrosion process. The high-frequency intercept on the real axis corresponds to the solution resistance (R_s), while the low-frequency intercept represents the charge transfer resistance (R_{ct}), a key indicator of the material's corrosion resistance. A notable trend in Figure 7 is the significant increase in the diameter of the semicircles upon the introduction of AA/MgAl LDH. This suggests an enhancement in charge transfer resistance (R_{ct}), implying that the composite effectively inhibits the corrosion process by forming a protective layer on the stainless steel surface. The impedance response changes with immersion time, demonstrating the composite's ability to sustain corrosion protection over extended periods.

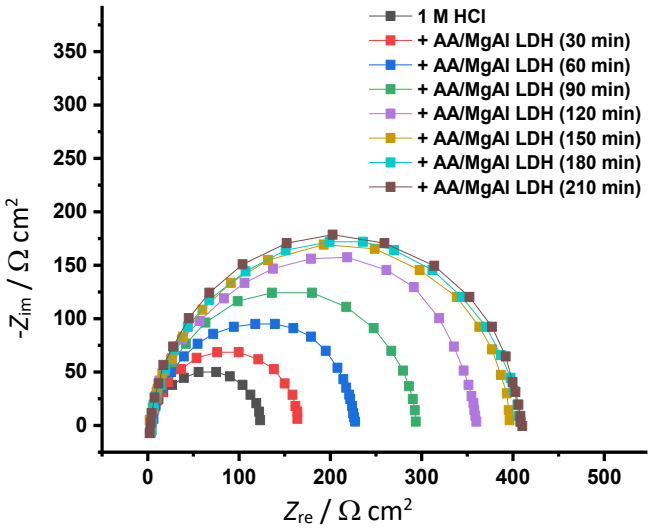

Figure 7. *Electrochemical impedance Nyquist spectra of stainless steel in 1 M HCl solution in the absence and presence of AA/MgAl LDH composite at different immersion times*

To quantitatively assess the impact of AA/MgAl LDH on corrosion inhibition, the Nyquist spectra were analysed using an equivalent circuit model $R_s(C_{dl}R_{ct})$ (Figure 8), commonly used to describe the stainless steel/acidic interface [48,49]. The fitting results, detailed in Table 2, confirm that the presence of the composite leads to a progressive increase in R_{ct}, suggesting its role as a corrosion inhibitor in an acidic medium. Nevertheless, these findings highlight the effectiveness of AA/MgAl LDH in mitigating stainless steel corrosion in 1 M HCl, with its inhibition performance improving over time.

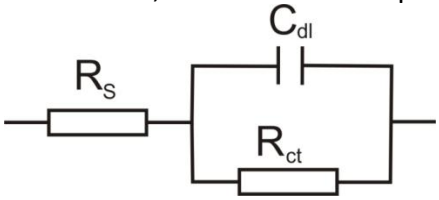

Figure 8. *Electrical equivalent circuit model*

As reported in previous studies, the incorporation of AA in the composite induces a significant reduction in double-layer capacitance (C_{dl}) compared to the uninhibited system (Table 2). According to the Helmholtz model, Equation (12):

$$C_{dl} = \frac{\varepsilon A}{\delta} \quad (12)$$

where ε is the absolute permittivity of the medium, A is the electrode surface area, and δ represents the thickness of the interfacial layer. The observed decrease in C_{dl} can be attributed to a reduction in the dielectric constant and/or an increase in the thickness of the double layer. This suggests that AA molecules, due to their adsorption capability, create a protective barrier over the corroding metal surface. The increase in R_{ct} with the presence of AA further supports the idea that AA/MgAl LDH forms a stable and adherent inhibitive film, effectively blocking active corrosion sites on stainless steel [50]. To quantify the corrosion inhibition performance of the composite, the inhibition efficiency (IE) (Table 2) was calculated using the relationship:

$$IE = \frac{R_{ct}(inh) - R_{ct}}{R_{ct}(inh)} 100 \quad (13)$$

Table 2. *Electrochemical impedance parameters of stainless steel in 1 M HCl solution in the absence and presence of AA/MgAl LDH composite at different immersion times*

Sample	Immersion time, min	C_{dl} / μFcm^{-2}	R_{ct} / Ω cm^2	IE, %
1 M HCl blank	-	28.080	124.008	-
1 M HCl blank + AA/MgAl LDH	30	20.200	165.731	25.17
	60	14.530	228.248	45.66
	90	11.007	295.417	58.02
	120	9.918	362.722	65.81
	150	8.094	396.785	68.74
	180	7.886	402.530	69.19
	210	7.731	410.054	69.75

Furthermore, the trend of C_{dl} values in 1 M HCl also reveals an important aspect of the inhibition mechanism. Within the initial 120 minutes, the compactness (or thickness) of the inhibitor film increases, suggesting that AA/MgAl LDH molecules progressively adsorb onto the stainless steel surface, forming a more effective barrier against aggressive chloride ions. This corresponds to a continuous increase in R_{ct} values, highlighting the enhancement of corrosion resistance. Beyond 120 minutes, C_{dl} continues to decrease, while R_{ct} keeps increasing, though at a slower rate. This indicates that the inhibitor layer reaches a saturation state, where most active sites on the steel surface are already covered by adsorbed inhibitor molecules. The continued decrease in C_{dl} suggests further film compaction, reinforcing the protective effect. Consequently, the inhibition efficiency stabilizes, demonstrating that the AA/MgAl LDH composite forms a durable and long-lasting barrier against corrosion without significant degradation over time. Moreover, the trend of inhibition efficiency aligns well with the observed evolution of R_{ct} and C_{dl}. Initially, as the inhibitor film becomes more compact, the corrosion resistance improves significantly, as reflected in the increasing R_{ct} values and decreasing C_{dl}. At longer immersion times, the protective layer reaches a saturation state, where further adsorption is minimal, but the film remains stable, continuing to provide effective corrosion resistance without significant degradation.

Thus, the inhibition mechanism follows a time-dependent behaviour: (i) early stage (0 to 120 min): progressive adsorption of AA molecules leads to increased inhibitor film compactness, reducing charge transfer and improving corrosion resistance, and (ii) saturation point (120 to 210 min), where the inhibitor layer reaches optimal compactness, offering maximum corrosion protection, as reflected in the

stabilization of IE. Overall, these findings demonstrate the strong and lasting potential of AA/MgAl LDH as a corrosion inhibitor in acidic environments, with its effectiveness stabilizing at prolonged immersion times rather than diminishing.

The Bode modulus ($|Z|$) and phase angle diagrams (Figures 9a and 9b) reveal three distinct frequency-dependent regions, which provide insights into the electrochemical behaviour of stainless steel in 1 M HCl in the presence and absence of the AA/MgAl LDH composite:

High-frequency region: in this region, log $|Z|$ remains nearly constant while the phase angle steadily falls toward 0°. This response is characteristic of a pure resistor, corresponding to the uncompensated solution resistance (R_s), which accounts for the resistance of the electrolyte between the reference and working electrodes. Similar behaviour has been previously reported in the literature [51,52].

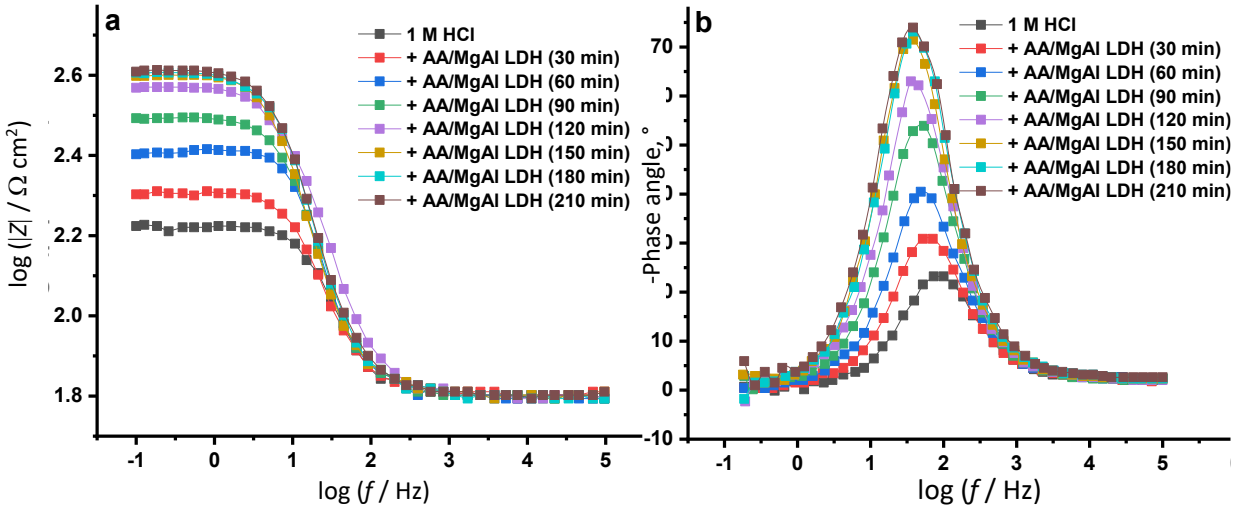

Figure 9. *Bode modulus (a) and phase angle plots (b) of stainless steel in 1 M HCl with and without AA/MgAl LDH composite at various immersion times*

Middle-frequency region: a linear variation of log $|Z|$ with log $|f|$ is observed, while the phase angle approaches a maximum near 80°. This is typical of a capacitive response, indicating the formation of a protective layer due to the adsorption of AA/MgAl LDH molecules on the stainless steel surface [51,52]. The observed phase angle peak reflects the time constant of the charge transfer process and the influence of the double-layer capacitance (C_{dl}), which is modified by inhibitor adsorption. The increase in phase angle in the presence of AA/MgAl LDH indicates a more compact and stable inhibitor layer, thereby enhancing corrosion protection.

Low-frequency region: at lower frequencies, log $|Z|$ reaches a plateau, remaining independent of log $|f|$, while the phase angle decreases again toward 0°. This corresponds to the charge transfer resistance (R_{ct})**,** which dominates the impedance response in the presence of corrosion inhibitors. The higher |Z| values observed at lower frequencies for the AA/MgAl LDH-treated samples confirm an increase in R_{ct}, correlating with improved corrosion resistance. The observed surface behaviour is characterized by a single relaxation process, as indicated by the single semicircle in the Nyquist plot and the single peak in the phase angle response [51,52]. This relaxation process is attributed to the charge transfer mechanism at the metal/electrolyte interface, modulated by the adsorbed AA/MgAl LDH inhibitor layer, which reduces the double-layer capacitance (C_{dl}) and enhances corrosion resistance.

These Bode plot observations align with the Nyquist plot trends (Figure 7) and electrochemical impedance parameters (Table 2). The well-defined capacitive behaviour in the middle-frequency

range and the sustained increase in impedance at low frequencies confirm the inhibitor's effectiveness in reducing charge transfer and corrosion rates.

Release mechanisms of AA species

The inhibition efficiencies corresponding to different immersion times were converted into a relative release rate using the electrolyte solution as a reference, allowing for a clearer understanding of the release kinetics of AA species from the MgAl LDH matrix. As depicted in Figure 10, the cumulative release profile exhibits a biphasic pattern: an initial rapid release phase within the first 120 min, followed by a slower, sustained release. Although MgAl LDH is thermodynamically unstable in harsh acidic conditions such as 1 M HCl, the observed release profile implies that dissolution is not immediate. The early burst is likely due to the desorption of loosely bound AA molecules from the outermost layers of the LDH structure, occurring primarily via ion exchange mechanisms, which ensure immediate availability of the inhibitor for corrosion protection. Beyond this period, the release rate decreases significantly, stabilizing at approximately 70 % cumulative release after 210 minutes. This slower phase suggests that AA molecules confined within the inner galleries of the LDH are released progressively as the host structure gradually degrades, indicating a strong host-guest interaction that supports sustained inhibitor delivery. Furthermore, the localized buffering effect from released OH^- ions, combined with the surface adsorption of AA, helps delay complete LDH dissolution, thereby extending corrosion protection throughout the immersion period. This correlates with the observed 70 % cumulative release, indicating that while most AA has been liberated, a residual fraction remains trapped within partially degraded or aggregated LDH structures.

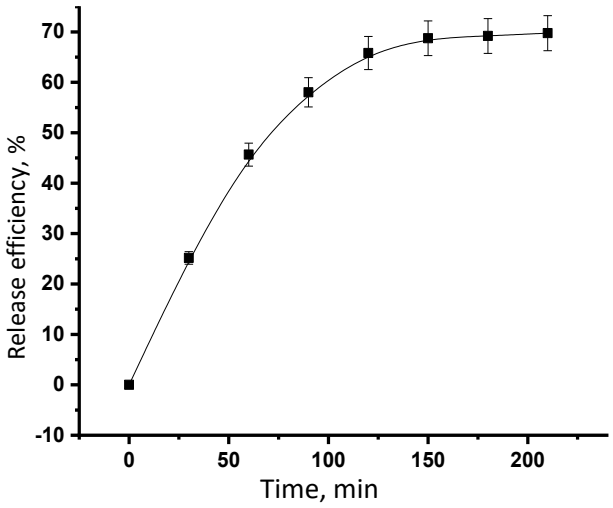

Figure 10. *Release profile of AA species from AA/MgAl LDH composite in 1 M HCl medium*

The correlation between the release profile and impedance data further supports the effectiveness of AA/MgAl LDH as a corrosion inhibitor. The initial rapid release corresponds to the progressive formation of the protective inhibitor layer, reflected in the increasing R_{ct} values and decreasing C_{dl}. As the release transitions into the sustained phase, the inhibitor film reaches its optimal compactness, stabilizing the corrosion resistance. This controlled release behaviour is a key factor in prolonging the inhibition effect over time, demonstrating the potential of AA/MgAl LDH as an efficient and durable anti-corrosion system in acidic environments.

To gain deeper insight into the release mechanism of AA species from the AA/MgAl LDH composite, three well-established kinetic models were employed: the zero-order model (Equation 14) [53,54], the first-order model (Equation 15) [54,55], and the Korsmeyer-Peppas model (Equation 16) [56]. These models help characterize the release profile and diffusion behaviour of AA species over time.

$$\frac{W}{W_0} = k_0 t \tag{14}$$

$$\ln\left(1 - \frac{W}{W_0}\right) = -k_1 t \tag{15}$$

$$\ln\left(\frac{W}{W_0}\right) = n \ln t + \ln k_{KP} \tag{16}$$

where W represents the amount of AA released at time t, W_0 is the initial amount of AA present at time zero, k_0, k_1, and k_{KP} are the release rate constants for the zero-order, first-order and Korsmeyer-Peppas models, respectively, and n is the diffusion exponent, which provides insights into the underlying release mechanism.

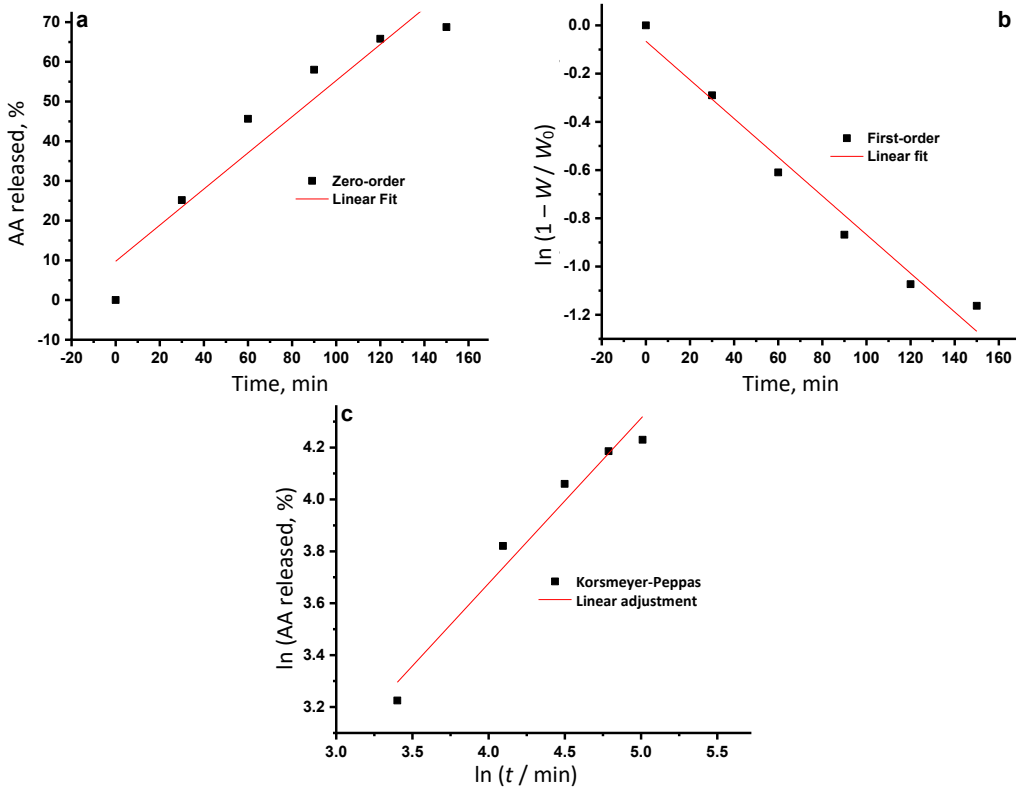

Figure 11. *Kinetic plots for AA release from AA/MgAl LDH composite*

By applying these kinetic models, we can assess whether the release of AA from the AA/MgAl LDH composite follows a constant rate (zero-order), a concentration-dependent rate (first-order), or a diffusion-controlled mechanism (Korsmeyer-Peppas). This analysis provides valuable insights into the controlled release behaviour of the composite. The kinetic parameters were derived using a linear fit approach and are presented in Table 3 for comparative analysis. Among the models tested, the Korsmeyer-Peppas model (Figure 11c) exhibits the highest determination coefficient (R^2 = 0.972), indicating that it best describes the AA release mechanism. The first-order model (Figure 11b) also exhibits a strong correlation (R^2 = 0.963), whereas the zero-order model (Figure 11a) displays a lower, yet still significant, R^2 value (0.912).

A key parameter of the Korsmeyer-Peppas model is the diffusion exponent (n = 0.636), which falls between 0.5 and 1.0. This range suggests that the release of AA follows a non-Fickian anomalous diffusion mechanism, meaning that it is governed by both diffusion and relaxational transport controlled by the LDH matrix. This behaviour indicates that the release process is not purely concentration-dependent but instead regulated by the structural properties of the LDH composite.

The high R^2 value for the zero-order model (>0.912) further confirms that the release process maintains a degree of independence from AA concentration, reinforcing the controlled and sustained nature of the release [54]. These findings align with prior research, particularly the tangible results obtained by Gasser *et al.* [46], further validating the LDH-controlled release mechanism. This suggests that the AA/MgAl LDH composite is an effective controlled-release system, capable of ensuring gradual and prolonged release of AA species, which is crucial for its application in corrosion inhibition and related fields.

Table 3. *Kinetic parameters for AA release from prepared AA/MgAl LDH composite*

	Zero-order	First-order	Korsmeyer-Peppas
R^2	0.912	0.963	0.972
n	-	-	0.636

Correlation between release kinetics and corrosion protection mechanisms

The release kinetics of AA from the AA/MgAl LDH composite strongly correlates with its corrosion inhibition performance, as evidenced by electrochemical impedance spectroscopy (EIS). The Korsmeyer-Peppas model (Figure 11c), which best describes the release mechanism, indicates a controlled and sustained diffusion process regulated by the LDH matrix, ensuring a steady supply of active species. This behaviour directly influences the time-dependent evolution of corrosion resistance, as seen in the impedance parameters (Table 2) and Bode plots (Figure 9). During the initial 120 min, AA species are progressively released and adsorbed onto the stainless steel surface, forming a compact and protective inhibitor film, reflected in the increase in R_{ct} and decrease in C_{dl}. Beyond 120 min, AA release slows but remains sustained, aligning with the stabilization of corrosion resistance, confirming that the inhibitor layer has reached optimal compactness. The non-Fickian diffusion mechanism (n = 0.636) further explains why the inhibition efficiency remains stable at ~70 % after 210 min preventing significant film degradation over time. Unlike conventional inhibitors prone to rapid depletion, the LDH matrix enables a long-lasting protective effect, ensuring continued adsorption and reinforcement of the corrosion barrier. Thus, the synergistic effect between controlled release and film integrity validates the superior performance of AA/MgAl LDH as a smart, self-regulating inhibitor for prolonged corrosion protection in acidic environments.

DFT calculations

MC simulations

To gain deeper insights into the adsorption mechanisms of ascorbic acid (AA) on both MgAl-LDH and iron surfaces, MC simulations were performed. The results of the geometry optimization are depicted in Figure 12, which presents the optimized molecular structures, while the adsorption energy (E_{ads}) values obtained from the simulations are listed in Table 4.

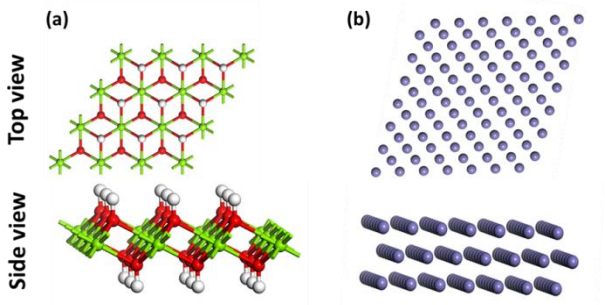

Figure 12. *Optimized structures of (a) the AA/MgAl LDH and (b) the AA/Fe(110) systems*

Table 4. *Adsorption energies (E_{ads}) of AA species on the MgAl LDH and Fe(110) surfaces*

System	Total energy, kJ mol^{-1}	E_{ads} / kJ mol^{-1}(E_{ads} / eV)
AA/MgAl LDH	-131.15	-723.07 (-4.73)
AA/Fe(110)	-50.00	-455.59 (-7.49)

The interaction between AA and the MgAl LDH surface is characterized by strong molecular affinity, as demonstrated by the short intermolecular distances observed post-optimization (Figure 13). This interaction is further supported by the highly negative adsorption energy of -723.07 kJ mol^{-1}, indicating a spontaneous and exothermic adsorption process. Similarly, for the AA/Fe system, the adsorption energy is approximately -455.59 kJ mol^{-1}, suggesting a thermodynamically favourable and stable interaction between ascorbic acid and the Fe surface. These findings underscore the potential of AA as an effective adsorbate on both MgAl LDH and Fe surfaces, with potential applications in surface modification and corrosion inhibition.

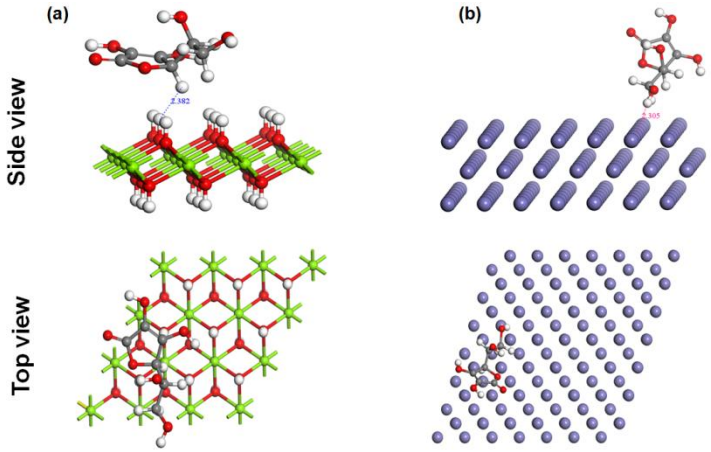

Figure 13. *The most stable adsorption configurations of the AA molecule on (a) MgAl LDH and (b) the Fe(110) surface, as determined by MC simulations*

MC simulations provided valuable insights into the adsorption behaviour of AA on both MgAl LDH and the Fe(110) surface of SS, revealing distinct interaction pathways (Figure 13). Based on the calculated adsorption energies and geometric parameters, both systems exhibit chemisorption, as confirmed by the significantly exothermic energies of -4.73 eV for AA/LDH and -7.49 eV for AA/Fe(110) (Table 4), which clearly exceed the conventional cut-off value of 1.0 eV used to distinguish physisorption from chemisorption. Moreover, the minimum distances between AA's reactive sites and the surface atoms are below 0.25 nm (0.2382 nm for AA/LDH and 0.2305 nm for AA/Fe(110)), consistent with strong bonding interactions. On the MgAl LDH surface, AA likely binds *via* hydrogen bonding between its -OH and C=O groups and surface hydroxyls, coordination to Mg^{2+}/Al^{3+}centres, and electrostatic interactions between negatively charged oxygen atoms and the positively charged LDH layers. Although hydrogen bonding is often associated with physisorption, the overall interaction energy indicates chemisorption, likely due to the combined effects of electrostatic attraction, hydrogen bonding, and partial charge transfer, which contribute to the stability of the AA/LDH complex. In contrast, adsorption on the Fe(110) surface is dominated by stronger chemisorption, involving the formation of coordination bonds between AA's oxygen atoms and Fe surface atoms, as well as π-d interactions between AA's conjugated π-system and the delocalized d-electrons of Fe. Additional stabilization may also arise from hydrogen bonding between the -OH and C=O functional groups of AA and surface hydroxyl groups (Fe-OH) formed by adsorbed water molecules. These strong and diverse interactions result in the formation of a tightly

bound, protective organic layer that effectively blocks the penetration of corrosive species (*e.g.* Cl^-, H^+), thereby enhancing corrosion resistance. Overall, the combination of high adsorption energies, short interaction distances, and the nature of the bonding confirms that AA is strongly anchored to both surfaces through chemisorption, promoting functional stability and surface passivation.

Electronic properties and reactivity indices

The analysis of quantum chemical parameters provides a comprehensive and detailed understanding of ascorbic acid (AA) as a corrosion inhibitor on the Fe surface. As indicated in Table 5, the electronegativity (χ) of AA, measured at 3.962 eV, supports its strong electron-accepting capability, suggesting that AA can effectively interact with the metal surface by donating electrons. The hardness (η) value of 3.880 eV indicates that AA is relatively stable and resistant to undergoing undesirable reactions, further reinforcing its potential as a corrosion inhibitor. The softness (σ) value of 0.257 eV highlights AA's moderate ability to donate electrons, facilitating its interaction with the metal surface. The electron affinity (A), defined as the molecule's ability to accept electrons and numerically equal to the negative of the LUMO energy, is 2.022 eV. This value supports the ability of AA to attract electron density from the metal surface during adsorption. Another key parameter is the electronic donation fraction (ΔN), which determines the direction and degree of electron transfer. According to this principle, electron transfer occurs from the element with lower electronegativity to the one with higher electronegativity to achieve chemical potential equilibrium. The positive ΔN of 0.391 eV value confirms that electron transfer occurs from the AA molecule to the Fe surface, with a greater magnitude than in the opposite direction. This confirms the donor-acceptor interaction between the metal and the AA molecule, leading to the formation of a protective surface layer and limiting the extent of corrosion.

Table 5. *Quantum chemical parameters of AA molecule*

Specie	E_{HOMO} / eV	E_{LUMO} / eV	ΔE_{gap} / eV	A / eV	χ / eV	η / eV	σ/ eV
AA	-5.902	-2.022	3.880	2.022	3.962	3.880	0.257

The HOMO-LUMO analysis (Figure 14) provides further insight into the adsorption mechanisms and the effectiveness of AA in corrosion inhibition. The highest occupied molecular orbital (HOMO) is responsible for electron donation, and its electron density is distributed across most of the AA molecule, with a significant concentration around the lactone ring, which serves as the primary electron-donating site. This homogenous distribution facilitates bonding on the metal surface and promotes the formation of a passive protective layer that minimizes the metal's susceptibility to corrosion by blocking reactive species from interacting with the surface. The electron density localized around the lactone ring highlights its crucial role in the inhibition process, ensuring a strong and effective interaction with the metal surface. Regarding the lowest unoccupied molecular orbital (LUMO), the electrostatic potential is predominantly concentrated around the lactone ring, suggesting that this region is likely the primary site for electron feedback from the metal surface to the AA molecule. Once electrons are donated from the HOMO, the metal surface can transfer some electron density back to the LUMO region of AA, stabilizing the adsorbed molecule. This electron feedback mechanism enhances the long-term stability and effectiveness of AA as a corrosion inhibitor by maintaining the integrity of the protective layer. Additionally, Mulliken charge distribution further clarifies how AA species interact with the metal surface. As shown in Table 6, the oxygen atoms in AA act as the primary nucleophilic sites, facilitating charge transfer to the metal surface and promoting effective adsorption. This charge transfer strengthens the protective effect by stabilizing the adsorbed layer, thereby enhancing surface passivation and improving corrosion resistance.

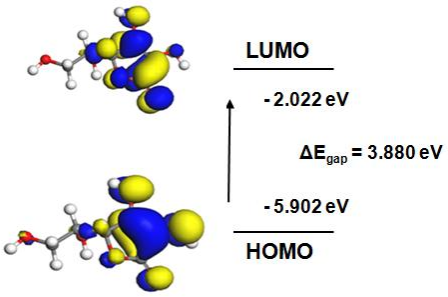

Figure 14. *Frontier molecular orbital density distributions HOMO and LUMO of AA*

Table 6. *Mulliken atomic charge distribution of AA molecule*

Atom	Mulliken charge	Atom	Mulliken charge	Atom	Mulliken charge	Atom	Mulliken charge
O (1)	-0.460	O (6)	-0.492	C (11)	0.192	H (16)	0.085
O (2)	-0.526	C (7)	0.056	C (12)	0.458	H (17)	0.306
O (3)	-0.492	C (8)	0.117	H (13)	0.152	H (18)	0.337
O (4)	-0.541	C (9)	0.269	H (14)	0.129	H (19)	0.309
O (5)	-0.520	C (10)	0.092	H (15)	0.097	H (20)	0.331

Reaction mechanisms

The inhibition of SS (Fe) corrosion by AA ($C_6H_8O_6$) in an HCl medium involves mainly adsorption and electrochemical processes (Figure 15). Below is a detailed explanation of the mechanisms:

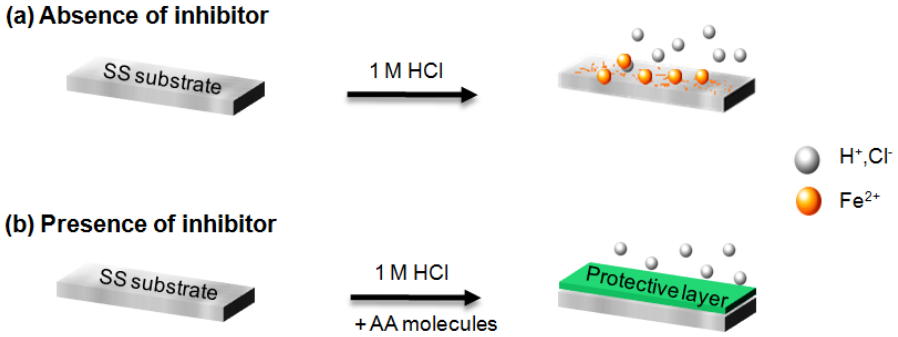

Figure 15. *SS substrate in the absence and presence of ascorbic acid as a corrosion inhibitor*

- In the absence of AA, Fe undergoes oxidation while H^+ ions are reduced:
  - Anodic reaction (iron dissolution): $Fe \rightarrow Fe^{2+} + 2e^-$
  - Cathodic reaction (hydrogen evolution): $2H^+ + 2e^- \rightarrow H_2\uparrow$
  - Overall corrosion reaction: $Fe + 2HCl \rightarrow FeCl_2 + H_2\uparrow$
- In the presence of AA, corrosion inhibition occurs through its effective adsorption onto the Fe surface, forming a protective layer that blocks aggressive species (H^+ and Cl^-): $Fe + C_6H_8O_6 \rightarrow \rightarrow (Fe{-}C_6H_8O_6)_{adsorbed}$. This adsorption involves both chemisorption, through the formation of coordination bonds between the oxygen atoms of AA (from -OH and C=O groups) and Fe surface atoms, and a secondary contribution from hydrogen bonding. The resulting adsorbed film serves as an effective physical and chemical barrier, hindering the diffusion of protons (H^+) and thereby reducing the cathodic hydrogen evolution reaction. It also prevents chloride ion (Cl^-) interaction with the surface, thus inhibiting $FeCl_2$ formation. These effects collectively suppress both anodic Fe dissolution and cathodic reactions, significantly enhancing corrosion resistance.

Furthermore, alongside the release of intercalated AA molecules directly at the SS surface, MgAl LDH provides corrosion protection through a dual mechanism, acting both as a sacrificial carrier and a localized pH buffer. In strongly acidic environments such as 1 M HCl, the LDH gradually dissolves,

releasing Mg^{2+}, Al^{3+} and hydroxide (OH^-) ions. The hydroxide ions neutralize nearby H^+ ions at the metal/solution interface, leading to a slight but significant local increase in pH, typically by 1-2 units, which substantially reduces the aggressiveness of the acidic medium and slows down corrosion kinetics. This localized pH modulation, often referred to as a "localized buffering effect" or "self-healing protection" [18], may also promote hydroxide precipitation, further enhancing corrosion resistance. Through this synergistic process, MgAl LDH creates a protective microenvironment that delays corrosion initiation and ensures prolonged inhibition performance even under highly aggressive acidic conditions.

Conclusion

In summary, this study demonstrates the effectiveness of AA intercalated into a MgAl layered LDH matrix as a sustainable corrosion inhibitor for stainless steel in an aggressive HCl environment. The AA/MgAl LDH composite, synthesized *via* the coprecipitation method, exhibited controlled release properties, leading to prolonged corrosion protection, as confirmed by XRD, FTIR, SEM, TEM, and EIS, with an inhibition efficiency of up to 70 % after 210 minutes in 1 M HCl. The release kinetics followed a non-Fickian diffusion mechanism, ensuring a sustained inhibitor supply and correlating with the progressive formation of a stable, compact protective layer on the steel surface. DFT calculations and MC simulations revealed strong interactions between AA, the LDH matrix, and the Fe surface, primarily driven by chemisorption, with contributions from hydrogen bonding and electrostatic forces, leading to enhanced adsorption and improved corrosion resistance. These findings highlight the AA/MgAl LDH composite as a smart, self-regulating inhibitor, integrating controlled release, strong interfacial interactions, and long-term protection, thus contributing to the development of environmentally friendly and efficient corrosion mitigation strategies.

Author contributions: *Amal Abdouli: Conceptualization, methodology and preparation, formal analysis, data collection, and DFT analysis. Mohamed Amine Djebbi: Data curation, supervision, writing original draft, review, and editing. Abdesslem Ben Haj Amara: Resources, funding acquisition, and validation. All authors have read and agreed to the published version of the manuscript.*

Competing interests: *The authors declare that they have no known competing financial interests or personal relationships that could be perceived to influence the work reported in this paper.*

Acknowledgement: *The authors would like to acknowledge all those who contributed their time and resources to the development of this work.*

References

[1] M. F. Ashby, *Materials Selection in Mechanical Design,* Butterworth-Heinemann, Elsevier Ltd, 2011, 1-13. https://doi.org/10.1016/B978-1-85617-663-7.00001-1

[2] L. T. Popoola, A. S. Grema, G. K. Latinwo, B. Gutti, A. S. Balogun, Corrosion problems during oil and gas production and its mitigation, *International Journal of Industrial Chemistry* **4** (2013) 35. https://doi.org/10.1186/2228-5547-4-35

[3] M. Schütze, *Handbook of Corrosion Engineering,* By P. R. Roberge, *McGraw*-Hill, New York - *Materials and Corrosion,* (2002) 284. https://doi.org/10.1002/1521-4176(200204)53:4<284::AID-MACO1111284>3.0.CO;2-8

[4] F. Aslani, M. Dehestani, Probabilistic impacts of corrosion on structural failure and performance limits of reinforced concrete beams, *Construction and Building Materials* **265**(2020)120316. https://doi.org/10.1016/j.conbuildmat.2020.120316

[5] H. Zhu, J. Li, Advancements in corrosion protection for aerospace aluminum alloys through surface treatment, *International Journal of Electrochemical Science* **19** (2024)100487. https://doi.org/10.1016/j.ijoes.2024.100487

[6] P. Boillota, J. Peultier, Use of stainless steels in the industry: recent and future developments, *Procedia Engineering* **83** (2014) 309-321. https://doi.org/10.1016/j.proeng.2014.09.015
[7] S. Narahari Prasad, M. Narayara Rao, Stainless steel - A versatile engineering material for critical applications, *Advanced Materials Research* **794** (2013)44-49. https://doi.org/10.4028/www.scientific.net/AMR.794.44
[8] P. Dhaiveegan, N. Elangovan, T. Nishimura, N. Rajendran, Corrosion behavior of 316L and 304 stainless steels exposed to industrial-marine-urban environment: field study, *RSC Advances* **6** (2016) 47314-47324. https://doi.org/10.1039/C6RA04015B
[9] R. G. Buchheit, H. Guan, S. Mahajanam, F. Wong, Active corrosion protection and corrosion sensing in chromate-free organic coatings, *Progress in Organic Coatings* **47** (2003) 174-182. https://doi.org/10.1016/j.porgcoat.2003.08.003
[10] M. Serdechnova, A. N. Salaka, F. S. Barbosa, D. E. L. Vieira, J. Tedim, M.L. Zheludkevich, M. G. S. Ferreira, Interlayer intercalation and arrangement of 2-mercaptobenzothiazolate and 1,2,3-benzotriazolate anions in layered double hydroxides:*In situ*X-ray diffraction study, *Journal of Solid State Chemistry* **233** (2016) 158-165. https://doi.org/10.1016/j.jssc.2015.10.023
[11] S. K. Poznyak, J. Tedim, L. M. Rodrigues, A. N. Salak, M. L. Zheludkevich, L. F. P. Dick, M. G. S. Ferreira, Novel inorganic host layered double hydroxides intercalated with guest organic inhibitors for anticorrosion applications, *ACS Applied Materials & Interfaces* **1** (2009) 2353-2362. https://doi.org/10.1021/am900495r
[12] M. L. Zheludkevich, J. Tedim, M. G. S. Ferreira, Smart coatings for active corrosion protection based on multi-functional micro and nanocontainers, *Electrochimica Acta* **82** (2012) 314-323. https://doi.org/10.1016/j.electacta.2012.04.095
[13] M. A. Djebbi, M. Braiek, S. Hidouri, P. Namour, N. Jaffrezic-Renault, A. Ben Haj Amara, Novel biohybrids of layered double hydroxide and lactate dehydrogenase enzyme: Synthesis, characterization and catalytic activity studies, *Journal of Molecular Structure* **1105** (2016) 381-388. https://doi.org/10.1016/j.molstruc.2015.10.065
[14] A. I. Khan, D. O'Hare, Intercalation chemistry of layered double hydroxides: recent developments and applications, *Journal of Materials Chemistry* **12** (2002)3191-3198. https://doi.org/10.1039/B204076J
[15] M. A. Djebbi, Z. Bouaziz, A. Elabed, M. Sadiki, S. Elabed, P. Namour, N. Jaffrezic-Renault, A. Ben Haj Amara, Preparation and optimization of a drug delivery system based on berberine chloride-immobilized MgAl hydrotalcite, *International Journal of Pharmaceutics* **506** (2016) 438-448. https://doi.org/10.1016/j.ijpharm.2016.04.048
[16] M. A. Djebbi, A. Elabed, Z. Bouaziz, M. Sadiki, S. Elabed, P. Namour, N. Jaffrezic-Renault, A. Ben Haj Amara, Delivery system for berberine chloride based on the nanocarrier ZnAl-layered double hydroxide: Physicochemical characterization, release behavior and evaluation of anti-bacterial potential, *International Journal of Pharmaceutics* **515** (2016) 422-430. https://doi.org/10.1016/j.ijpharm.2016.09.089
[17] N. Bakhtaoui, O. Benali, E. Mazarío, F. J. Recio, P.Herrasti, Layered double hydroxides intercalated with methyl orange as a controlled-release corrosion inhibitor for iron in chloride media, *Nano Express* **2** (2021) 010017. https://doi.org/10.1088/2632-959X/abe2b6
[18] A. C. Bouali, M. Serdechnova, C. Blawert, J. Tedim, M. G. S. Ferreira, M. L. Zheludkevich, Layered double hydroxides (LDHs) as functional materials for the corrosion protection of aluminum alloys: A review, *Applied Materials Today* **21** (2020) 100857. https://doi.org/10.1016/j.apmt.2020.100857
[19] C. Jing, B. Dong, A. Raza, T. Zhang, Y. Zhang, Corrosion inhibition of layered double hydroxides for metal-based systems, *Nano Materials Science* **3** (2021) 47-67. https://doi.org/10.1016/j.nanoms.2020.12.001

[20] M. V. Phan, T. K. T. Tran, Q. N. Pham, M. H. Do, T. H. N. Nguyen, M. T. Nguyen, T. T. Phan, T. X. H. To, Controllable synthesis of layered double hydroxide nanosheets to build organic inhibitor-loaded nanocontainers for enhanced corrosion protection of carbon steel, *Nanoscale Advances* **6** (2024) 606. https://doi.org/10.1039/D3NA00570D

[21] R. C. Zeng, Z. G. Liu, F. Zhang, S. Q. Li, H. Z. Cui, E. H. Han, Corrosion of molybdate intercalated hydrotalcite coating on AZ31 Mg alloy, *Journal of Materials Chemistry A* **2** (2014) 13049-13057. https://doi.org/10.1039/C4TA01341G

[22] Y. Sui, X. Liu, S. Bai, X. Li, Z. Sun, Phosphate loaded layered double hydroxides for active corrosion protection of carbon steel, *Corrosion Engineering Science and Technology* **57** (2022) 7-14. https://doi.org/10.1080/1478422X.2021.1976086

[23] R. Fuchs-Godec, M. G. Pavlović, M. V. Tomić, The inhibitive effect of vitamin-C on the corrosive performance of steel in HCl solutions, *International Journal of Electrochemical Science* **8** (2013)1511-1519. https://doi.org/10.1016/S1452-3981(23)14115-0

[24] M. A. Chidiebere, E. E. Oguzie, L. Liu, Y. Li, F. Wang, Corrosion inhibition of Q235 mild steel in 0.5 M H_2SO_4solution by phytic acid and synergistic iodide additives, *Industrial & Engineering Chemistry Research* **53** (2014) 7670-7679. https://doi.org/10.1021/ie404382v

[25] B. D. F. Souza, M. R. Lage, A. Oliveira dos Santos, F. Ferreira de Sousa, R. Gester, S. R. Stoyanov, T. Andrade-Filho, Ascorbic acid, ascorbate, and dehydroascorbic acid as green corrosion inhibitors: A computational investigation, *Corrosion and Materials Degradation* **5** (2024) 615-623. https://doi.org/10.3390/cmd5040029

[26] X. Gao, L. Lei, D. O'Hare, J. Xie, P. Gao,T. Chang, Intercalation and controlled release properties of vitamin C intercalated layered double hydroxide, *Journal of Solid State Chemistry* **203** (2013)174-180. https://doi.org/10.1016/j.jssc.2013.04.028

[27] N. Ben Smida, M. A. Djebbi, C. Hmimen, S. Elabed, A. Ben Haj Amara, R. Abderrahim, Exploring an efficient approach for Hg^{2+} ion detection in water using a glassy carbon electrode modified with bistriazinone: Experimental methods and DFT computational insights, *Journal of The Electrochemical Society* **172** (2025) 067525. https://doi.org/10.1149/1945-7111/ade47e

[28] R. Wang, D. Wang, X. Wang, W. Peng, Y. Wang, J. Zhang, Experimental and DFT study of F^-removed by Cl^--hydrotalcite, *New Journal of Chemistry* **46** (2022) 12290-12299. https://doi.org/10.1039/D2NJ01360F

[29] E. S. Zhitova, R. M. Sheveleva, A. V. Kasatkin, A. A. Zolotarev, V. N. Bocharov, A. N. Kupchinenko, D. I. Belakovski, Crystal structure of hydrotalcite group mineral—desautelsite, $Mg_6Mn^{III}_2(OH)_{16}(CO_3)4H_2O$, and relationship between cation size and in-plane unit cell parameter, *Symmetry* **15** (2023) 1029. https://doi.org/10.3390/sym15051029

[30] K. Mahmoud, M. Taha, A. Zaher, R. M. Amin, Understanding the physicochemical properties of Zn-Fe LDH nanostructure as sorbent material for removing of anionic and cationic dyes mixture, *Scientific Reports* **11** (2021) 21365. https://doi.org/10.1038/s41598-021-00437-w

[31] B. Zhang, S. Yuan, D. Sun, Y. Li,T. Wu, Experimental and theoretical calculation investigation of 2,4-dichlorophenoxyacetic acid adsorption onto core-shell carbon microspheres@layered double hydroxide composites, *RSC Advances* **8** (2018) 856. https://doi.org/10.1039/C7RA11138J

[32] C. Hmimen, A. Elabed, S. Boubakri, M. A. Djebbi, A. Ben Haj Amara, S. Ibnsouda Koraichi, S. Elabed, Synergistic effects of activated carbon and MgZnAl layered triple hydroxides for removing anionic and cationic dyes: Experimental and theoretical insights, *Chemical Engineering Science* **309** (2025) 121409. https://doi.org/10.1016/j.ces.2025.121409

[33] P. P. Ewald, The calculation of optical and electrostatic lattice potentials, *Annals of Physics* **369** (1921) 253-287. https://doi.org/10.1002/andp.19213690304

[34] X. Ding, K. Chang, J. Tian, Y. Yang, W. Jiao, Y. Hou, Z. Zeng, Z. Huang, Effects of pore structures and multiple components in flue gas on the adsorption behaviors of dioxins by

activated carbon, *Colloids and Surfaces A: Physicochemical and Engineering Aspects* **661** (2023) 130868. https://doi.org/10.1016/j.colsurfa.2022.130868

[35] Z. Huang, C. Xiong, L. Ying, W. Wang, S. Wang, J. Ding, J. Lu, Facile synthesis of a MOF-derived magnetic CoAl-LDH@chitosan composite for Pb (II) and Cr (VI) adsorption, *Chemical Engineering Journal* **449** (2022) 137722. https://doi.org/10.1016/j.cej.2022.137722

[36] H. Cheng, H. He, Z. Zhang, K. Xiao, Y. Liu, X. Kang, Y.Lu, X.Kang, X. Li, Adsorption sites and electron transfer characteristics of methyl orange on three-dimensional hierarchical flower-like nanostructures of Co-Al-layered double hydroxides: Experimental and DFT investigation, *Separation and Purification Technology* **303** (2022) 122282. https://doi.org/10.1016/j.seppur.2022.122282

[37] M. Khnifira, W. Boumya, J. Attarki, A. Mahsoune, M. Sadiq, M. Abdennouri, S. Kaya, N. Barka, A combined DFT, Monte Carlo, and MD simulations of adsorption study of heavy metals on the carbon graphite (111) surface, *Chemical Physics Impact* **5** (2022) 100121. https://doi.org/10.1016/j.chphi.2022.100121

[38] M. A. Djebbi, M. Braiek, P. Namour, N. Jaffrezic-Renault, A. Ben Haj Amara, Layered double hydroxide materials coated carbon electrode: New challenge to future electrochemical power devices, *Applied Surface Science* **386** (2016) 352-363. https://doi.org/10.1016/j.apsusc.2016.06.032

[39] R. Chitrakar, S. Tezuka, A. Sonoda, K. Sakane, T. Hirotsu, A new method for synthesis of Mg-Al, Mg-Fe, and Zn-Al layered double hydroxides and their uptake properties of bromide ion, *Industrial & Engineering Chemistry Research* **47** (2008) 4905-4908. https://doi.org/10.1021/ie0716417

[40] J. T. Feng, X. Ma, Y. He, D. G. Evans, D. Q. Li, Synthesis of hydrotalcite-supported shape-controlled Pd nanoparticles by a precipitation-reduction method, *Applied Catalysis A: General* **413-414** (2012) 10-20. https://doi.org/10.1016/j.apcata.2011.10.034

[41] Y. Tang, X. Zhang, X. Li, J. Bai, C. Yang, Y. Zhang, Z. Xu, X. Jin, Y. Jiang, Facile synthesis of magnetic ZnAl layered double hydroxides and efficient adsorption of malachite green and congo red, *Separation and Purification Technology* **322** (2023) 124305. https://doi.org/10.1016/j.seppur.2023.124305

[42] V. Rives, *Layered double hydroxides: Present and future,* Nova Science Publishers Inc., New York, USA, 2001. ISBN 978-1-61209-289-8

[43] Y. Kameshima, H. Sasaki, T. Isobe, A. Nakajima, K. Okada, Synthesis of composites of sodium oleate/Mg-Al-ascorbic acid-layered double hydroxides for drug delivery applications, *International Journal of Pharmaceutics* **381** (2009) 34-39. https://doi.org/10.1016/j.ijpharm.2009.07.021

[44] D. Williams, L. H. Rogers, The infrared absorption spectrum of vitamin C, *Journal of the American Chemical Society* **59** (**1937)** 1422-1423. https://doi.org/10.1021/ja01287a005

[45] J. H. Choy, Y. H. Son, Intercalation of vitamer into LDH and their controlled release properties, *Bulletin of the Korean Chemical Society* **25** (2004) 122-126. https://doi.org/10.5012/bkcs.2004.25.1.122

[46] M. S. Gasser, Inorganic layered double hydroxides as ascorbic acid (vitamin C) delivery system—Intercalation and their controlled release properties, *Colloids and Surfaces B* **73** (2009) 103-109. https://doi.org/10.1016/j.colsurfb.2009.05.005

[47] D. G. Evans, X. Duan, Preparation of layered double hydroxides and their applications as additives in polymers, as precursors to magnetic materials and in biology and medicine, *Chemical Communications* **42** (2006) 485-496. https://doi.org/10.1039/B510313B

[48] Z. Tao, S. Zhang, W. Li, B. Hou, Corrosion inhibition of mild steel in acidic solution by some oxo-triazole derivatives, *Corrosion Science* **51** (2009) 2588-2595. https://doi.org/10.1016/j.corsci.2009.06.042

[49] M. Kissi, M. Bouklah, B. Hammouti, M. Benkaddour, Establishment of equivalent circuits from electrochemical impedance spectroscopy study of corrosion inhibition of steel by pyrazine in sulphuric acidic solution, *Applied Surface Science* **252** (2006) 4190-4197. https://doi.org/10.1016/j.apsusc.2005.06.035

[50] R. A. Prabhu, T. V. Venkatesha, A. V. Shanbhag, B. M. Praveen, G. M. Kulkarni, R. G. Kalkhambkar, Quinol-2-thione compounds as corrosion inhibitors for mild steel in acid solution, *Materials Chemistry and Physics* **108** (2008) 283-289. https://doi.org/10.1016/j.matchemphys.2007.09.038

[51] H. Gerengi, M. M. Mielniczek, G. Gece, M. M. Solomon, Experimental and quantum chemical evaluation of 8-hydroxyquinoline as a corrosion inhibitor for copper in 0.1 M HCl, *Industrial and Engineering Chemistry Research* **55** (2016) 9614-9624. https://doi.org/10.1021/acs.iecr.6b02414

[52] M. Finšgar, B. Petovar, K. Xhanari, U. Maver, The corrosion inhibition of certain azoles on steel in chloride media: Electrochemistry and surface analysis, *Corrosion Science* **111** (2016) 370-381. https://doi.org/10.1016/j.corsci.2016.05.028

[53] R. S. Soumya, S. Ghosh, E. T. Abraham, Preparation and characterization of guar gum nanoparticles. *International Journal of Biological Macromolecules* **46** (2010) 267-269. https://doi.org/10.1016/j.ijbiomac.2009.11.003

[54] S. Mondal, S. Dasgupta, K. Maji, MgAl-Layered double hydroxide nanoparticles for controlled release of salicylate, *Materials Science and Engineering C* **68** (2016) 557-564. https://doi.org/10.1016/j.msec.2016.06.029

[55] F. Li, L. Jin, J. Han, M. Wei, C. Li, Synthesis and controlled release properties of prednisone intercalated Mg−Al layered double hydroxide composite, *Industrial and Engineering Chemistry Research* **48** (2009) 5590-5597. https://doi.org/10.1021/ie900043r

[56] R. W. Korsmeyer, R. Gurny, E. Doelker, P. Buri, N. A. Peppas, Mechanisms of solute release from porous hydrophilic polymers, *International Journal of Pharmaceutics* **15** (1983) 25-35. https://doi.org/10.1016/0378-5173(83)90064-9